Unveiling the Different Physical Origin of Magnetic Anisotropy and Magnetoelasticity in Ga-rich FeGa Thin Films

P. Bartolomé[1], A. Begué[2], A. Muñoz-Noval[1], M. Ciria[2], and R. Ranchal[1,3 *]

[1]*Dpto. Física de Materiales, Facultad de Ciencias Físicas. Universidad Complutense de Madrid. Ciudad Universitaria s/n, Madrid 28040, Spain*

[2]*Instituto de Ciencia de Materiales de Aragón, Consejo Superior de Investigaciones Científicas, Zaragoza, Spain, and Departamento de Física de la Materia Condensada, Universidad de Zaragoza, Zaragoza, Spain*

[3]*Instituto de Magnetismo Aplicado, UCM-ADIF-CSIC, Las Rozas, Spain*

ABSTRACT

The aim of this work is to clarify how the in-plane magnetic anisotropy and magnetoelasticity depend on the thickness of Ga-rich FeGa layers. Samples with a $Fe_{72}Ga_{28}$ composition were grown by sputtering in the ballistic regime in oblique incidence. Although for these growth conditions uniaxial magnetic anisotropy could be expected, in-plane anisotropy is only present when the sample thickness is above 100 nm. By means of differential x-ray absorption spectroscopy we have determined the influence of both Ga-pairs and tetragonal cell distortion on the evolution of the magnetic anisotropy with the increase of FeGa thickness. On the other hand, we have used the cantilever beam technique with capacitive detection to also determine the evolution of the magnetoelastic parameters with the thickness increase. In this case, experimental results can be understood considering the grain distribution. Therefore, the different physical origin for anisotropy and magnetoelasticity opens the possibility of independently tune these two characteristics in Ga-rich FeGa films.

Corresponding author.

* Dr. R. Ranchal

Dpto. Física de Materiales, Facultad de CC. Físicas. Ciudad Universitaria s/n

Madrid 28040, Spain

rociran@ucm.es

Introduction

Magnetic anisotropy, that can have many different origins, is one of the fundamental parameters of magnetic materials[1]. Except the shape magnetic anisotropy, the rest of anisotropies depend on interactions at the atomic level[1-2]. Therefore, the understanding of the origin of this parameter is crucial for the control and development of advanced magnetic materials. Magnetostriction is the phenomenon in which the shape of a magnetic material changes during its magnetization process, and it is quantified through the parameter λ which is defined as:

$$\lambda = \frac{l-l_0}{l} = \frac{\Delta l}{l} \quad (1)$$

where l and l_0 are the final and initial dimensions, respectively, in a certain direction[1]. As magnetic anisotropy, the magnetostriction originates in the interaction between the magnetic moments at the atomic level. Moreover, they are closely related since the magnetostriction constants can be obtained from the derivative of the anisotropy.

In the last years, the metallic FeGa system has attracted a huge interest due to the discovery in 2000 of a large magnetostriction in these free rare-earth alloys[3-4]. Many of the published works have been devoted to the understanding of the origin of this enhanced magnetostriction in contrast with pure Fe[5-15]. It is remarkable that the largest deformation in Fe can be reached in the [100] direction with a $(3/2)\lambda_{100}$ value of 45 ppm[16], whereas in FeGa alloys reaches up to 430 ppm[7]. The investigations of FeGa thin films have shown the strong impact that the different structural orderings from long to local range have on the magnetic properties of these alloys[6, 17-24]. Closely related to these investigations are those about the origin of the magnetic anisotropy in either in the plane or in the out of plane directions of FeGa thin films[5, 11, 21, 23-27]. There is still some controversy about the origin of magnetoelasticity in FeGa with works pointing to an intrinsic effect[7-8], or to nanoheterogeneities that induce some tetragonal distortion of the matrix[12]. In the case of

magnetic anisotropy, it seems that Ga-pairs and/or tetragonal distortion play an important role[21, 23-24, 26].

Since largest values of magnetostriction are obtained in the so-called second peak of magnetostriction, we have focused our study on FeGa alloys in the Ga-rich range (28 at. %)[21, 23-24]. Previously, it has been found that the magnetic anisotropy can vanish when the thickness is low enough[23]. In this work, we have performed an exhaustive investigation on the evolution of the magnetic anisotropy due to Ga-Ga pairing and tetragonal distortion with the layer thickness. For this study, we have employed a combination of linear dichroism (LD) in the x-ray absorption near edge structure (XANES) spectroscopy and differential extended x-ray absorption fine structure (Diff-EXAFS) spectroscopy. The latter is a technique that allows to detect subtle structural distortions as small as 10^{-4} Å[16-17]. In this work, we have employed LD-XANES and Diff-EXAFS to qualitatively compare the Ga-Ga pairing and tetragonal distortion at the atomic level in the FeGa structure as a function of the film thickness. To detect these differences we have measured the FeGa thin films with a linearly polarized monochromatic x-ray beam in two different directions: with the polarization vector close to be parallel to the surface normal, and close to be perpendicular to the surface normal. Later on, these two measurements are subtracted. The subtracted signal, commonly named dichroic is analyzed considering two regions: the region close to the edge gives the LD-XANES, and the region that corresponds to the EXAFS is threated here as a Diff-EXAFS.

On the other hand, to clarify whether magnetic anisotropy and magnetoelasticity have a common physical origin, we have performed magnetoelastic (ME) stress measurements for FeGa films with different thickness. Our experimental results indicate

that whether anisotropy can be understood considering local range order, Ga pairs and tetragonal distortion, magnetoelasticity seems to be related to grains distribution.

Experimental Section

$Fe_{72}Ga_{28}$ layers were grown by the DC magnetron sputtering technique in the ballistic regime at room temperature on glass substrates capped with 20-nm thick Mo layers. A 20-nm thick Mo layer was also used as a capping layer to avoid oxidation. Mo buffers and cappings were grown with a power of 90 W and with an Ar pressure of 3×10^{-3} mbar. The deposition was carried out in oblique incidence with an angle between the vapor beam and the perpendicular to the sample of about 25° and a distance of 9 cm between target and substrate. This direction of the vapor beam within the sample plane is taken as the reference direction to control the direction of the in-plane uniaxial anisotropy axis when created[21, 23-24, 28]. The $Fe_{72}Ga_{28}$ films were deposited from a target with a composition of $Fe_{72}Ga_{28}$ with a diameter of 5 cm and a thickness of 2 mm using an Ar pressure of 3×10^{-3} mbar and a growth power of 50 W in all cases. In order to avoid effects related to the target ageing, the samples were deposited consecutively.

At room temperature, in-plane hysteresis loops were carried out in a vibrating sample magnetometer (VSM). In the VSM we can rotate the sample being possible to measure the in plane loops at different angles between the applied magnetic field and the in-plane reference direction taken as the beam incidence direction in the sample plane.

X-ray absorption spectroscopy (XAS) experiments were performed at BL22-CLAESS beamline in ALBA synchrotron (Spain). The spectra were acquired at the Fe and Ga K-edges (7112 eV and 10367 eV, respectively) in fluorescence yield mode. At least 3 scans were acquired and merged for each polarization, edge and sample. By this

procedure the energy drifts due to x-ray optics instabilities are minimized. XAS data were reduced applying standard procedures using the Demeter package[29]. In the normal incidence (NI) measurements, the polarization vector forms a 5° angle respect to the surface, whilst in the grazing incidence (GI), the polarization vector forms a 85° angle with respect to the surface plane. The LD-XANES and the Diff-EXAFS spectrum is obtained from the subtraction of XAS spectra with GI and NI for each sample, and the comparison for films with different thickness and identical composition provide the information about Ga-Ga pairing and tetragonal distortion.

ME stress measurements were performed by means of a cantilever beam technique with capacitive detection. The substrate and the thin film are clamped by one end covering an electrode with fixed dimensions as is described elsewhere[30]. By evaluating the difference of ME stress (σ_{ME}) with the magnetic field parallel and transverse to the cantilever beam, an effective ME stress B_{eff} can be obtained. Knowledge of the crystalline orientation allow to relate B_{eff} with irreducible ME stresses[30]. A magnetic field of 1 kG, generated by a dipole magnet, is rotated via a stepping motor; this value for the applied magnetic field is strong enough to assume saturation of the film along any in-plane direction. The deflection of the beam is obtained as a function of the angle φ formed by the cantilever length and the magnetic field. The system has been calibrated on thick epitaxial Fe(100) films grown on MgO(001) substrates by using known values of the cubic B_1 and B_2 ME coefficients[31] as reference. Corning glass substrates with thickness 250 μm, Young's modulus 77 GPa and Poisson ratio 0.21 was used to obtain $\sigma_{ME}(\varphi)$.

Results and Discussion

The in-plane hysteresis loops in fig. 1 illustrate the evolution of the in-plane magnetic anisotropy as a function of the thickness. FeGa layers with a thickness of 25

and 50 nm show an isotropic behavior. In the 100 nm layer, a rather small uniaxial magnetic anisotropy is observed being this anisotropy fully developed for a 150 nm. This is in accordance with a previous work in which a clear in-plane magnetic anisotropy for a layer with 250 nm thickness was observed, whereas a 30 nm-thick layer was isotropic[23]. As also previously reported, the uniaxial magnetic easy axis appears in the direction of the beam incidence in the sample plane[21, 23-24].

Diff-XAS has been proved to be a powerful technique to characterize the local structure of Fe-based alloys[16-18, 21, 23-24, 32-34]. The LD-XANES provides a tool to study the local structure in the FeGa thin films[23], particularly from the information obtained at the Ga K-edge. The features in the LD-XANES at Ga K-edge have been previously attributed to the existence of both Ga-pairs and tetragonal cell distortion of the cubic structure[23]. In figure 2 we present the LD-XANES spectra as a function of the FeGa thickness. The negative peak ca. 10.37 keV is a signature of Ga-Ga pairing, in such a way that the larger the peak the higher the relative amount of Ga-pairs. Therefore, the enhancement of the negative peak with the increase of the thickness is an indication of the increase of Ga-pairs in the sample plane as the FeGa layer becomes thicker. The second feature in the LD-XANES spectra, at 10.39 keV, is assigned to the tetragonal distortion of the cubic unit cell caused by the transition from A2 to B2 phase[23]. This tetragonal distortion is reflected in the LD-XANES as a maximum (Fig.2). This second feature is clearly distinct in the sample with the highest thickness with also a clear in-plane magnetic anisotropy. Thus, the tetragonal cell distortion in the sample plane in comparison to the out of plane direction observed in the Ga K-edge is higher in the thickness for which the in-plane magnetic anisotropy is fully developed[23]. Therefore, the critical thickness for the crossover between isotropy to anisotropy lies between 100 and 150 nm FeGa thickness, being related to the enhancement of both Ga-pairs and tetragonal cell distortion.

It should be noted that these are subtracted spectra that provide qualitative information. Further evidences about the cell distortion are provided by the Diff-EXAFS signals (χ(E)) shown in figure 3. According to Pettifer *et al.*[17], Diff-EXAFS gives information about the structural distortion even for variations in the femtometre-scale in the local structure (better than 10^{-4} Å). The EXAFS signal can be expressed as a composition of the scattering paths: $\chi(k) = \sum A(j)\sin(kS_j + \phi_j(k))$, and thus, the Diff-EXAFS can be obtained by a first-order Tailor expansion: $\Delta\chi(k) = \sum A(j)\cos(kS_j + \phi_j(k))2k\Delta R$. Here k is the photoelectron wave number, *A(i)* the *i*- scattering path function, $S(i)$ the scattering path distance, $\phi_j(k)$ the phase of the photoelectron, and ΔR the variation of the scattering path that causes the variation in the EXAFS signal ($\Delta\chi(k)$). The Diff-EXAFS signal has a phase shift of $\pi/2$ with respect to the EXAFS, and an additional k weight which results in an enhancement of the signal at higher energies, and therefore, a sensitivity to farther atomic neighbors. The most important feature in the Diff-EXAFS signal is the amplitude that is proportional to the variation of the scattering path (or the variation of the atomic neighbor distances). As shown in figure 3a, corresponding to the Ga K-edge Diff-EXAFS spectra, the thicker the layer the clearer and more intense the Diff-EXAFS oscillations become. The EXAFS spectrum of the 150 nm layer in the NI configuration is also shown to observe the $\pi/2$ phase shift and verify the observable oscillations at high energies. Therefore, this also probes the distortion of the cubic cell in accordance with the signs observed in LD-XANES.

The Fe K-edge Diff-EXAFS has provided additional information about the cell distortion (fig. 3b). It has been previously observed the increase of the Debye-Waller factor (σ^2) calculated for the Fe K-edge when there was a uniaxial easy axis in the sample plane[23]. In this work, the Diff-EXAFS spectra in the Fe K-edge show a progressive decrease of the oscillations amplitude as the FeGa layers become thicker. Even though

the increase in the cell distortion might produce an increase in the Diff-EXAFS amplitude in the Fe K-edge, the effect of the increase in the local disorder perceived by the Fe in the whole FeGa structure is probably more relevant. Other sources for the magnetic anisotropy related to oblique deposition Some additional origins to the magnetic anisotropy might be the angle of deposition, internal stress, miscut of substrates, ... However, we have used the same angle, Ar pressure, growth power, and substrate for all the layers studied in this work. Therefore, we can rule out these sources as the origin for the observed dependence between the magnetic anisotropy and thickness in the samples presented in this work.

Once we have determined the correlation between Ga pairs and cell distortion on the evolution of the magnetic anisotropy of films with increasing FeGa thickness, it is also crucial to determine the evolution of the magnetoelastic properties. Figure 4.a shows several plots of $\sigma_{ME}(\varphi)$ for films with thickness 12 nm, 100 nm and 250 nm. The dependence of B_{eff} with the film thickness is presented in figure 4b where it is shown that the modulus of B_{eff} decreases as the film thickness increases. Therefore, a first direct conclusion is that the thickness increase has a different effect on the magnetoelasticity in comparison to the magnetic anisotropy.

For polycrystalline films, the effective ME stress B_{eff} can be related to the irreducible B_1 and B_2 stresses assuming a certain distribution for the orientation of individual crystallites. The films studied here present a (110) texture as observed in sputtered layers deposited under the same growth conditions[21,23], so in the coordinate system with *x* || [110], y || [$\underline{1}$10] z|| [001] the ME energy reads:

$$e_{ME} = B_1\left[\left(\alpha_z^2 - \frac{1}{3}\right)\left(\varepsilon_{zz} - \frac{\varepsilon_{xx}+\varepsilon_{yy}}{2}\right) + 2\alpha_x\,\alpha_y\,\varepsilon_{xy}\right] + B_2\left[\frac{1}{2}\left(\alpha_x^2 - \alpha_y^2\right)\left(\varepsilon_{xx} - \varepsilon_{yy}\right) + 2\alpha_x\,\alpha_z\,\varepsilon_{zx} + 2\alpha_z\,\alpha_y\,\varepsilon_{yz}\right] \quad (2)$$

Where ε_j and α_j are strain components and direction cosine of the magnetization, respectively. Considering a random distribution for the in-plane directions, the averaged ME energy yields $\langle B_{eff} \rangle = -(3B_1 + 5B_2)/8$, and for Ga 28 at. %, B_1 = -5 MPa and B_2 = -12.5 MPa[35], it is obtained $\langle B_{eff} \rangle$ = -9.7 MPa. For the thinner films, 12 nm and 25 nm, B_{eff} is around or larger than the value predicted by the isotropic distribution of grains while above 100 nm, B_{eff} is about -7.5 MPa. The thickness dependence of ME coefficients in epitaxial thin films is usually explained by considering surface or second order strain effects[35]. However, no significant variation for B_1 and B_2 with respect to the bulk values has been reported for FeGa epitaxial films[15]. On the other hand, because B_{eff} can be expressed in terms of the crystallite axis distribution, changes of the values of the magnetostriction can be related to variations in the crystal texture of the films[36]. This consideration can be applied straightforward to the films studied here since deviations from the random distribution for the in-plane crystallite direction can result in the weakening of $|\langle B_{eff} \rangle|$.

To argument this point we consider σ_{ME} for a single crystallite with the [001] direction along the beam direction $B_{[100]}$. Obtaining σ_{ME} in terms of B_1 and B_2 requires setting to zero the stress perpendicular to the film plane[35], and ε_{xx} becomes related the in-plane strains ε_{yy} and ε_{zz}. Thus, $B_{[100]} = B_1 (1 + c/2)$ where $c = 2c_{12}/(c_{11} + c_{12} + 2c_{44})$, a ratio between the film elastic constants. The value of c is evaluated by using for c_{11}, c_{12}, and c_{44} values measured for a crystal with Ga 27.2 at. %[37], obtaining c = 0.39 and getting $B_{[100]}$ = -6 MPa. We note that $\langle B_{eff} \rangle$ does not include ratios of elastic constants because for a polycrystal that kind of contribution does not change with the azimuthal angle. Therefore, an increment of the proportion of [001]-grains shifts the value of B_{eff} from $\langle B_{eff} \rangle$ to $B_{[100]}$ decreasing the value obtained by assuming a random distribution of grains.

If grains with ME contribution that goes with B_2 are predominant in the structure, an increment of B_{eff} will be expected.

Therefore, while the magnetic anisotropy seems to be related to the local range order (Ga pairs and tetragonal distortion) in Ga-rich $Fe_{100-x}Ga_x$ alloys, the magnetoelastic behavior can be understood considering the distribution of grains, i.e. medium range order. This result goes in the same direction than a previous report on Barturen *et al*.[15] in epitaxial $Fe_{100-x}Ga_x$ thin films with a Ga content near 19 at. %. Furthermore, our experimental results show for the first time the possibility of independently controlling magnetic anisotropy and magnetoelasticity in FeGa thin films.

Conclusion

In summary, we have studied the evolution of the in-plane magnetic anisotropy and magnetoelasticity as a function of the thickness in sputtered Ga-rich FeGa thin films. With XAS experimental results and employing spectra differential analysis, including LD-XANES and Diff-EXAFS, we have probed the correspondence of the Ga-pairs and tetragonal distortion with the appearance of in-plane magnetic anisotropy for a thickness above 100 nm in the FeGa layers. On the other hand, magnetoelasticity is related to the grain distribution, i.e. medium range order. Therefore, this work represents a fundamental step in the control of the magnetic properties of this family of alloys in order to integrate the material system in advanced magnetic devices such as recently proposed strain controlled devices[14, 38].

Acknowledgements. We thank ALBA synchrotron for providing time and technical assistance at BL22 beamline, and Instituto of Sistemas Optoelectrónicos y

Microtecnología (ISOM) for using some of its facilities. This work has been financially supported through the projects MAT2015-66888-C3-3-R and MAT2015-66726-R (MINECO/FEDER) of the Spanish Ministry of Economy and Competitiveness, RTI2018-097895-B-C43 of the Spanish Ministry of Science, Innovation, and Universities, and Gobierno de Aragón (Grant E10-17D) and Fondo Social Europeo. A. M.-N. thanks the contract from Universidad Complutense and Comunidad de Madrid "Atracción de Talento" program 2018-T1/IND-10360, and A. B. thanks MINECO for the Ph. D. grant BES-2016-076482.

References

[1] Chikazumi, S.; Graham, Jr C. D. *Physics of Magnetism*, Oxford University Press, **1997**

[2] du Trémolet de Lacheisserie, E. *Magnétisme*. EDP Sciences, **2000**.

[3] Clark, A. E.; Restorff, J.B.; Wun-Fogle, M.; Lograsso, T.A.; Schlagel, D.L. Magnetostrictive properties of body-centered cubic Fe-Ga and Fe-Ga-Al alloys. *IEEE Trans. Magn*. **2000**, *36*, 3238−3240.

[4] Clark, A. E.; Wun-fogle, M.; Lograsso, T. A.; Cullen, J. R. Effect of quenching on the magnetostriction of $Fe_{1-x}Ga_x$ ($0.13 < x < 0.21$). *IEEE Trans. Magn.* **2001**, *37*, 2678-2680.

[5] Cullen, J.; Zhao, P.; Wuttig, M. Anisotropy of crystalline ferromagnets with defects. *J. Appl. Phys.* **2007**, *101*, 123922

[6] Pascarelli, S.; Ruffoni, M. P.; Sato Turtelli, R.; Kubel, F.; Grössinger, R. Local structure in magnetostrictive melt-spun $Fe_{80}Ga_{20}$ alloys. *Phys. Rev. B* **2008**, *77*, 184406.

[7] Xing, Q.; Du, Y.; McQueeney, R.J.; Lograsso, T.A. Structural investigations of Fe-Ga alloys: phase relations and magnetostrictive behavior. *Acta Mater*. **2008**, *56*, 4536−4546.

[8] Wu, R. Origin of large magnetostriction in FeGa alloys. *J. Appl. Phys.* **2002**, *91*, 7358.

[9] Laver, M.; Mudivarthi, C.; Cullen, J. R.; Flatau, A. B.; Chen, W. C.; Watson, S. M.; Wuttig, M. Magnetostriction and magnetic heterogeneities in iron-gallium. *Phys. Rev. Lett.* **2010**, *105*, 027202.

[10] Atulasimha, J; Flatau, A. B. A review of magnetostrictive iron–gallium alloys *Smart Mater. Struct.* **2011**, *20*, 043001.

[11] Basumatary, H.; Palit, M.; Arout Chelvane, J.; Arvindha Babu, D.; Sarkar, R.; Pandian, S. Microstructure and magnetostriction of melt-spun $Fe_{73}Ga_{27}$ ribbon. *Appl. Phys. Lett.* **2012**, *101*, 144106.

[12] He, Y.; Ke, X.; Jiang, C.; Miao, N.; Wang, H.; Coey, J. M. D.; Wang, Y.; Xu, H. Interaction of trace rare-earth dopants and nanoheterogeneities induces giant magnetostriction in Fe-Ga alloys. *Adv. Funct. Mater.* **2018**, *28* 1800858.

[13] He, Y. K.; Jiang, C. B.; Wu, W.; Wang, B.; Duan, H.; Wang, H.; Zhang, T.; Wang, J.; Liu, J.; Zhang, Z.; Stamenov, P.; Coey, J. M. D.; Xu. H. Giant heterogeneous magnetostriction in Fe–Ga alloys: effect of trace element doping. *Acta Mater*. **2016**, *109*, 177-186.

[14] Ahmad, H.; Atulasimha, J.; Bandyopadhyay, S. Reversible strain-induced magnetization switching in FeGa nanomagnets: pathway to a rewritable, non-volatile, non-toggle, extremely low energy straintronic memory. *Sci. Rep.* **2015**, *5*, 18264.

[15] Barturen, M.; Sander, D.; Milano, J.; Premper, J.; Helman, C.; Eddrief, M.; Kirschner, J.; Marangolo, M. Bulklike behavior of magnetoelasticity in epitaxial $Fe_{1-x}Ga_x$ thin films. *Phys. Rev. B* **2019**, *99*, 134432.

[16] Xing, Q.; Lograsso, T. A.; Ruffoni, M. P.; Azimonte, C.; Pascarelli, S.; Miller, D. J. Experimental exploration of the origin of magnetostriction in single crystalline iron. Appl. Phys. Lett. **2010**, *97*, 072508.

[17] Pettifer, R. F.; Mathon, O.; Pascarelli, S.; Cooke, M. D.; Gibss, M. R. J. Measurement of femtometre-scale atomic displacements by X-ray absorption spectroscopy. *Nature* **2005**, *435*, 78-81.

[18] Ruffoni, M. P.; Pascarelli, S.; Grössinger, R.; Turtelli, R. S.; Bormio-Nunes, C.; Pettifer, R. F. Direct measurement of intrinsic atomic scale magnetostriction. *Phys. Rev. Lett.* **2008**, *101*, 147202.

[19] Arenholz, E.; van der Laan, G.; McClure, A.; Idzerda, Y. Electronic and magnetic structure of Ga_xFe_{1-x} thin films. *Phys. Rev. B* **2010**, *82*, 180405.

[20] Eddrief, M.; Zheng, Y.; Hidki, S.; Rache Salles, B.; Milano, J.; Etgens, V. H.; Marangolo, M. Metastable tetragonal structure of $Fe_{100-x}Ga_x$ epitaxial thin films on ZnSe/GaAs(001) substrate. *Phys. Rev. B* **2011**, *84*, 161410.

[21] Muñoz-Noval, A.; Ordóñez-Fontes, A.; Ranchal, R. Influence of the sputtering flow regime on the structural properties and magnetic behavior of Fe-Ga thin films (Ga ∼30 at.%). *Phys. Rev. B* **2016**, *93*, 214408.

[22] Ciria, M.; Proietti, M. G.; Corredor, E. C.; Coffey, D.; Begué, A.; de la Fuente, C.; Arnaudas, J. I.; Ibarra, A. Crystal structure and local ordering in epitaxial $Fe_{100-x}Ga_x$/MgO(001) films. *J. Alloys Compd.* **2018**, *767*, 905−914

[23] Muñoz-Noval, A.; Fin, S.; Salas-Colera, E.; Bisero, D.; Ranchal, R. The role of surface to bulk ratio on the development of magnetic anisotropy in high Ga content Fe100-xGax thin films. *J. Alloys Compd.* **2018**, *745*, 413−420.

[24] Muñoz-Noval, A.; Fin, S.; Salas-Colera, E.; Bisero, D.; Ranchal, R. Local and medium range order influence on the magnetic behavior of sputtered Ga-rich FeGa thin films. *J. Phys. Chem. C* **2019**, *123*, 13131-13135.

[25] Barturen, M.; Rache Salles, B.; Schio, P.; Milano, J.; Butera, A.; Bustingorry, S.; Ramos, C.; de Oliveira, A. J. A.; Eddrief, M.; Lacaze, E.; Gendron, F.; Etgens, V. H.; Marangolo, M. Crossover to striped magnetic domains in $Fe_{1-x}Ga_x$ magnetostrictive thin films. *Appl. Phys. Lett.* **2012**, *101*, 092404.

[26] Barturen, M.; Milano, J.; Vasquez-Mansilla, M.; Helman, C.; Barral, M. A.; Llois, A. M.; Eddrief, M.; Marangolo, M. Large perpendicular magnetic anisotropy in magnetostrictive $Fe_{1-x}Ga_x$ thin films. *Phys. Rev. B* **2015**, *92*, 054418.

[27] Ranchal, R.; Fin, S; D. Bisero, D. Magnetic microstructures in electrodeposited $Fe_{1-x}Ga_x$ thin films ($15 \leq x \leq 22$ at.%). *J. Phys. D: Appl. Phys.* **2015**, *48*, 075001.

[28] Maicas, M.; Ranchal, R.; Aroca, C.; Sánchez, P.; López, E. Magnetic properties of permalloy multilayers with alternating perpendicular anisotropies. *Eur. Phys. J. B* **2008**, *62*, 267−270.

[29] Ravel, B.; Newville, M. ATHENA, ARTEMIS, HEPHAESTUS: Data analysis for X-ray absorption spectroscopy using IFEFFIT. *J. Synchrotron Radiat.* **2005**, *12*, 537−541.

[30] Ciria, M.; Arnaudas, J. I.; Benito, L.; de la Fuente, C.; del Moral, A.; Ha, J. K.; O'Handley, R. C. Magnetoelastic coupling in thin films with weak out-of-plane anisotropy. *Phys. Rev. B* **2003**, *67*, 024429.

[31] Wedler, G.; Walz, J.; Greuer, A.; Koch, R. Stress dependence of the magnetoelastic coupling constants B_1 and B_2 of epitaxial Fe(001). *Phys. Rev. B* **1999**, *60*, R11313-R11316.

[32] Harris, V. G.; Aylesworth, K. D.; Das, B. N.; Elam, W. T.; Koon, N. C. Structural origins of magnetic anisotropy in sputtered amorphous Tb-Fe films. *Phys. Rev. Lett.* **1992**, *69*, 1939-1942.

[33] Harris, V. G.; Pokhil, T. Selective-resputtering-induced perpendicular magnetic anisotropy in amorphous TbFe films. *Phys. Rev. Lett.* **2001**, *87*, 067207.

[34] Pascarelli, S.; Ruffoni, M. P.; Trapananti, A.; Mathon, O.; Detlefs, C.; Pasquale, M.; Magni, A.; Sasso, C. P.; Celegato, F.; Olivetti, E.; Joly, Y.; Givord, D. 4f charge-density deformation and magnetostrictive bond strain observed in amorphous $TbFe_2$ by x-ray absorption spectroscopy. *Phys Rev. B* **2010**, *81*, 020406.

[35] Sender, D. The correlation between mechanical stress and magnetic anisotropy in ultrathin films. *Rep. Prog. Phys.* **1999**, *62*, 809-858.

[36] Jahjah, W.; Manach, R.; Le Grand, Y.; Fessant, A.; Warot-Fonrose, B.; Prinsloo, A. R. E.; Sheppard, C. J.; Dekadjevi, D. T.; Spenato D.; Jay, J.-Ph. Thickness dependence

of magnetization reversal and magnetostriction in $Fe_{81}Ga_{19}$ thin films. *Phys. Rev. Appl.* **2019**, *12*, 024020.

[37] Clark, A. E.; Hathaway, K. B.; Wun-Fogle, M.; Restorff, J. B.; Lograsso, T. A.; Keppens, V. M. Extraordinary magnetoelasticity and lattice softening in bcc Fe-Ga alloys. *J. Appl. Phys.* **2003**, *93*, 8621-8623.

[38] Foerster, M.; Macià, F.; Statuto, N.; Finizio, S.; Hernández-Mínguez, A.; Lendínez, S.; Santos, P. V.; Fontcuberta, J.; Hernàndez, J. M.; Kläui, M.; Aballe, L. Direct imaging of delayed magneto-dynamic modes induced by surface acoustic waves. Nature Comm. **2017**, *8*, 407.

Figure captions

Figure 1. Room temperature hysteresis loops recorded with the applied magnetic field in the sample plane for as-grown FeGa layers with different thickness: (a) 25 nm, (b) 50 nm, (c) 100 nm, and (d) 150 nm. The hysteresis loops are measured considering 0° the beam incidence direction.

Figure 2. LD-XANES spectra obtained from the subtraction of the GI with respect to NI spectra for FeGa layers of increasing thickness for the Ga K-edge.

Figure 3. Diff-EXAFS spectra obtained from the subtraction of the GI with respect to NI spectra for FeGa layers of increasing thickness for (a) the Ga K-edge, and (b) the Fe K-edge.

Figure 4. (a) Detail of ME stress obtained by rotating the sample by π radians. The applied field is turn a number n of times around the sample. B_{eff} is obtained with B along ($\varphi = n\pi$) and transverse ($\varphi = (n/2)\pi$) to the cantilever beam. (b) B_{eff} vs film thickness.

Figure 1.

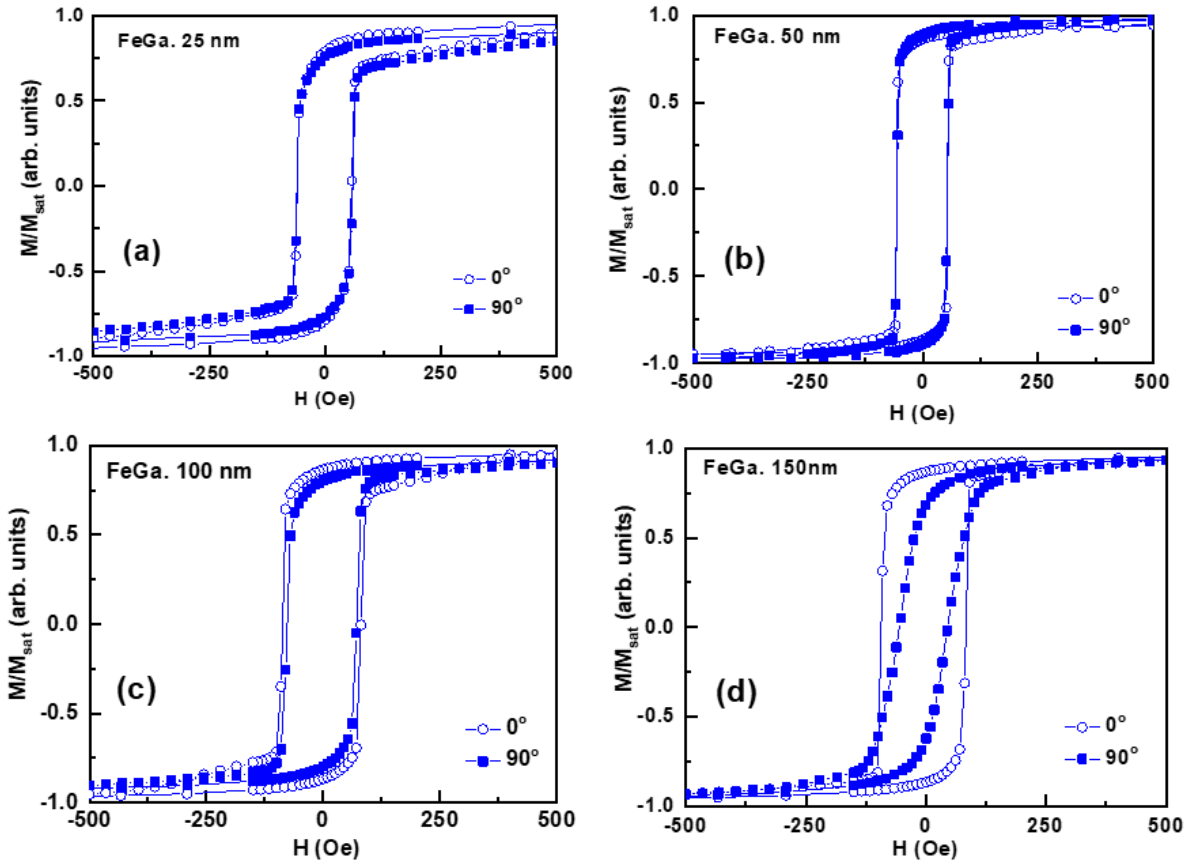
FeGa. 25 nm
(a)
FeGa. 50 nm
(b)
FeGa. 100 nm
(c)
FeGa. 150nm
(d)
M/M$_{sat}$ (arb. units)
H (Oe)
0°
90°
1.0
0.5
0.0
-0.5
-1.0
-500
-250
0
250
500

Figure 2.

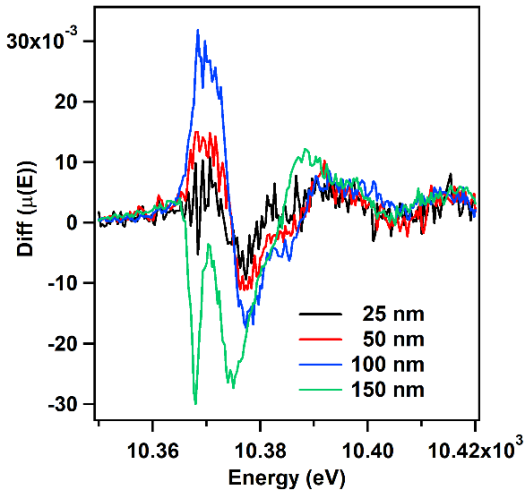
30x10-3
20
10
0
-10
-20
-30
Diff (μ(E))
10.36
10.38
10.40
10.42x103
Energy (eV)
25 nm
50 nm
100 nm
150 nm

Figure 3.

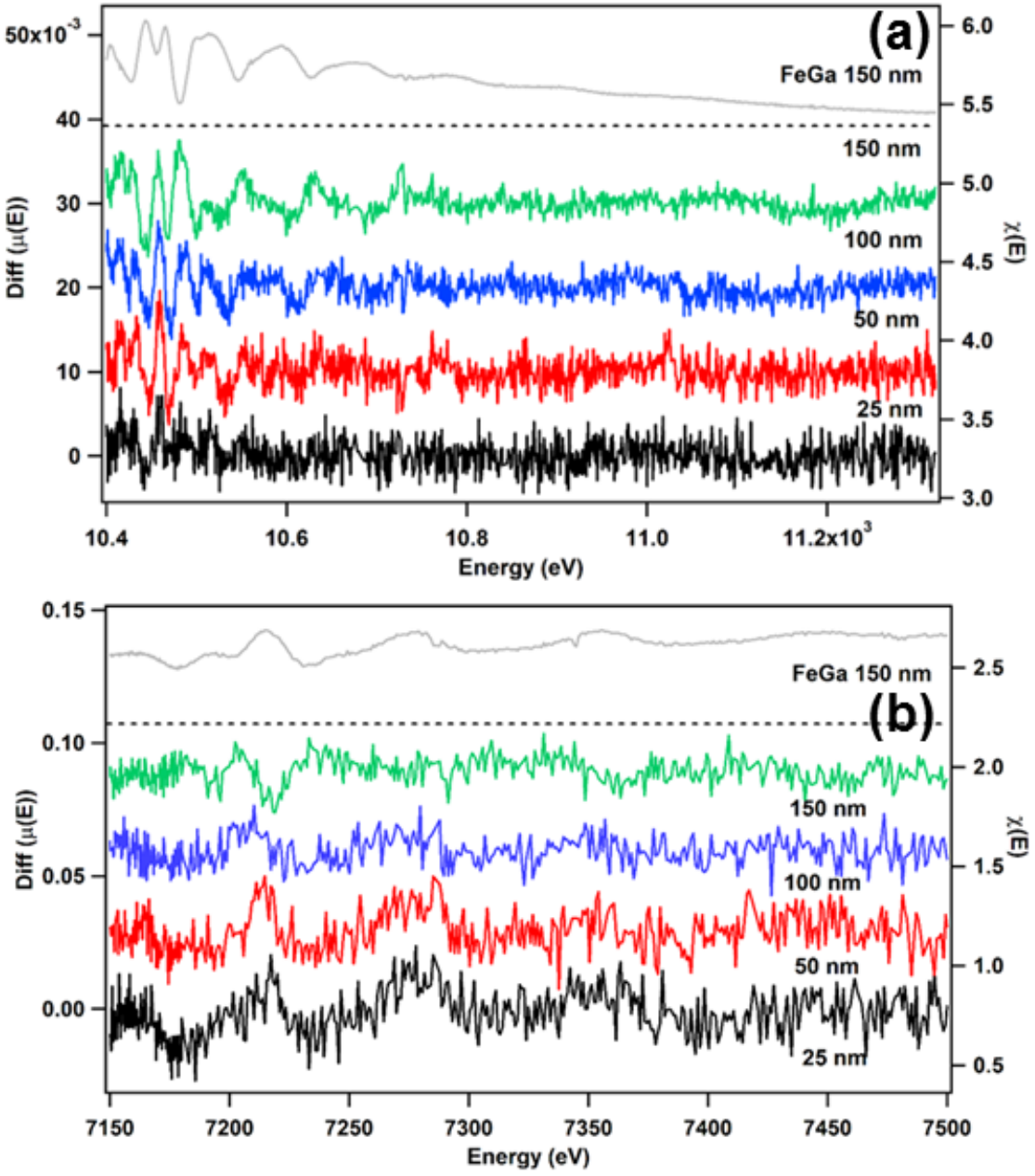
(a)
FeGa 150 nm
150 nm
100 nm
50 nm
25 nm
50x10^-3
40
30
20
10
0
Diff (μ(E))
6.0
5.5
5.0
4.5
4.0
3.5
3.0
χ(E)
10.4
10.6
10.8
11.0
11.2x10^3
Energy (eV)
(b)
FeGa 150 nm
150 nm
100 nm
50 nm
25 nm
0.15
0.10
0.05
0.00
Diff (μ(E))
2.5
2.0
1.5
1.0
0.5
χ(E)
7150
7200
7250
7300
7350
7400
7450
7500
Energy (eV)

Figure 4.

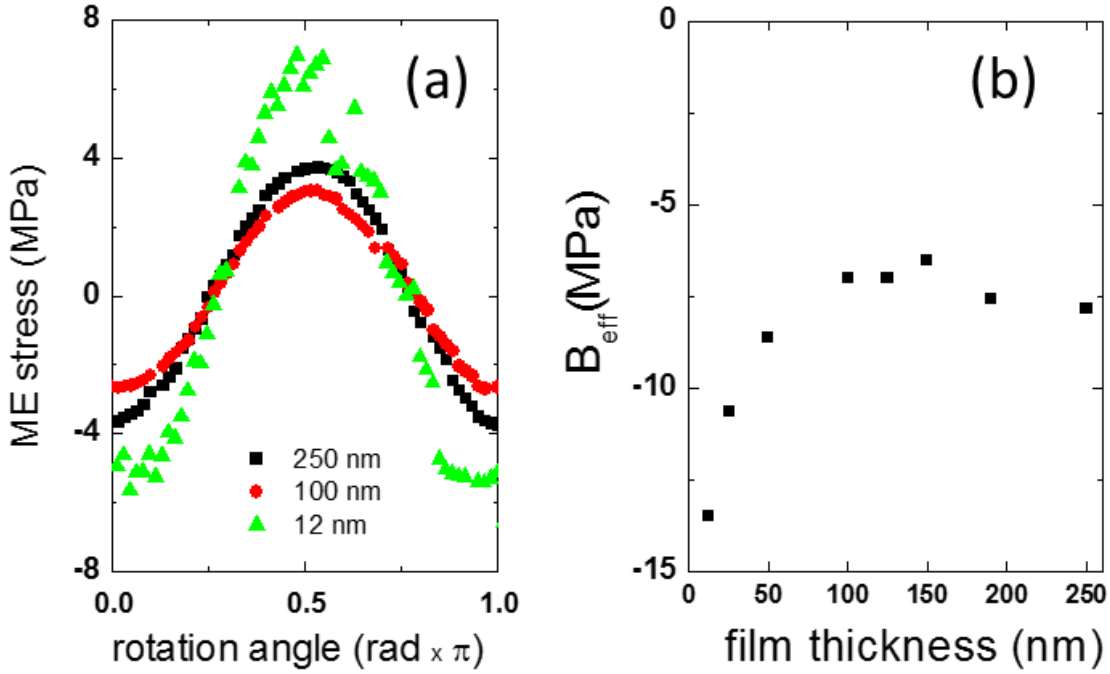
(a)
ME stress (MPa)
8
4
0
-4
-8
0.0
0.5
1.0
rotation angle (rad x π)
250 nm
100 nm
12 nm
(b)
B_eff (MPa)
0
-5
-10
-15
0
50
100
150
200
250
film thickness (nm)

TOC Graphic

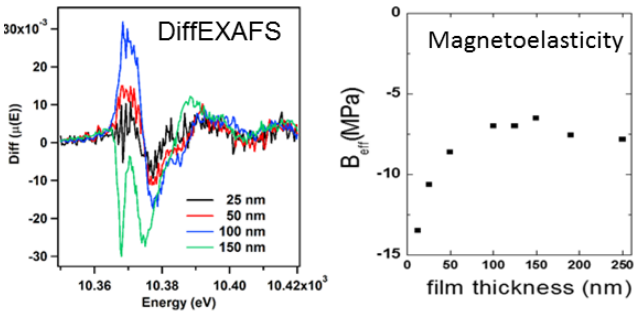
DiffEXAFS
30x10-3
20
10
0
-10
-20
-30
Diff (μ(E))
25 nm
50 nm
100 nm
150 nm
10.36
10.38
10.40
10.42x10^3
Energy (eV)
Magnetoelasticity
0
-5
-10
-15
Beff (MPa)
0
50
100
150
200
250
film thickness (nm)